Available online at www.sciencedirect.com

jmr&t Journal of Materials Research and Technology

www.jmrt.com.br

Original Article

Magnetic and microwave properties of $SrFe_{12}O_{19}/MCe_{0.04}Fe_{1.96}O_4$ (M = Cu, Ni, Mn, Co and Zn) hard/soft nanocomposites

N.A. Algarou[a,b], Y. Slimani[a], M.A. Almessiere[a,*], F.S. Alahmari[c], M.G. Vakhitov[d,e], D.S. Klygach[d,e], S.V. Trukhanov[d,f], A.V. Trukhanov[d,f,g], A. Baykal[c]

[a] Department of Biophysics, Institute for Research and Medical Consultations (IRMC), Imam Abdulrahman Bin Faisal University, P.O. Box 1982, 31441, Dammam, Saudi Arabia

[b] Department of Physics, College of Science, Imam Abdulrahman Bin Faisal University, P.O. Box 1982, 31441, Dammam, Saudi Arabia

[c] Department of Nanomedicine Research, Institute for Research and Medical Consultations (IRMC), Imam Abdulrahman Bin Faisal University, P.O. Box 1982, 31441, Dammam, Saudi Arabia

[d] South Ural State University, 454080, 76, Lenin Prospekt, Chelyabinsk, Russia

[e] Ural Federal University, 620002, 19 Mira street, Ekaterinburg, Russia

[f] SSPA Scientific and Practical Materials Research centre of the NAS of Belarus, 220072, 19 Brovki str., Minsk, Belarus

[g] NUST MISIS, 119049, 4, Leninsky ave., Moscow, Russia

ARTICLE INFO

Article history:
Received 27 February 2020
Accepted 28 March 2020
Available online 27 April 2020

Keywords:
Hard/soft
Structure
Citrate sol-gel approach
Magnetic properties
Exchange-coupling behavior
Microwave properties

ABSTRACT

This paper reports the synthesis, structural characteristics and magnetism of $SrFe_{12}O_{19}/MCe_{0.04}Fe_{1.96}O_4$ (M = Cu, Ni, Mn, Co and Zn) hard/soft nanocomposites. The hard/soft compositions were manufactured via a *one-pot* reactions citrate sol-gel approach. The hard/soft phases formation was confirmed using XRD, SEM, TEM and HRTEM techniques. *M vs. H* (Magnetization measurements) were done at unbent temperature and 10 K. Smoothed *M* against *H* loops and single peaks in *dM/dH vs. H* curves were noticed in $SrFe_{12}O_{19}/MnCe_{0.04}Fe_{1.96}O_4$, $SrFe_{12}O_{19}/CuCe_{0.04}Fe_{1.96}O_4$ and $SrFe_{12}O_{19}/ZnCe_{0.04}Fe_{1.96}O_4$ hard/soft nanocomposites. This indicated the manifestation of well exchange-coupled effect among hard and soft phases in these composites. However, $SrFe_{12}O_{19}/CoCe_{0.04}Fe_{1.96}O_4$ and $SrFe_{12}O_{19}/NiCe_{0.04}Fe_{1.96}O_4$ hard/soft nanocomposites showed non-well smoothed *M* against *H* loops and two peaks in *dM/dH* versus *H* plots, indicating that the dipolar interactions are unimportant compared to exchange-coupling behavior. Among all prepared nanocomposites, the $SrFe_{12}O_{19}/MnCe_{0.04}Fe_{1.96}O_4$ hard/soft nanocomposite showed the highest exchange-coupling behavior. Microwave properties of the $SrFe_{12}O_{19}/MCe_{0.04}Fe_{1.96}O_4$ (M = Cu, Ni, Mn, Co and Zn) hard/soft nanocomposites were investigated using coaxial method with applied frequency values fall between 2 and 18 GHz. Reflection losses were calculated from frequency dependences of the imaginary and real parts of permeability and permittivity. The correlation between the chemical composition of the spinel phase (A-cation) and microwave properties of composites. Most intensive electromagnetic

* *Corresponding author.*
E-mail: malmessiere@iau.edu.sa (M. Almessiere).

https://doi.org/10.1016/j.jmrt.2020.03.113

absorption was observed for Ni- and Mn-spinels. This is can be a result of the differences in electron shell configuration and radii for A-site ions in the spinel phase. Change of the absorption mechanisms (transition from ionic polarization to dipole polarization) was observed.

1. Introduction

In modern technology, magnetic metal oxides are playing a prominent role because of their outstanding physical properties and potential applications in the area of nanoscience and nanotechnology [1,2]. For magnetism, due to relative high Curie temperature, excellent corrosion resistance, their low cost, high electrical resistivity and minor size with unique physical and chemical features, metal ferrites in their both forms; spinel ferrite (as soft) and hexaferrite (as hard) are talented for advanced permanent magnetic materials [3,4]. For spinel ferrites, their high chemical and thermal stability, non-toxicity, economic efficiency and high saturation magnetization (M_s), make them multifunctional materials applied in various fields such as biomedicine, catalysis, magnetic recording, and sensing [5–7]. However, the spinel ferrite nanoparticles are possessing low coercivity (H_c) [8]. On the other hand, hexaferrite nanoparticles are exhibiting large coercivity. High-performance magnets are characterized by high magnetization and high coercivity, simultaneously, which are accomplished by nanocomposites soft/hard ferrite nanoparticles [9]. The combination between soft and hard ferrites may produce new material called exchange-spring magnets, which have improved coercivity and magnetization [10,11]. According to Kneller and Hawig [10], when hard and soft phases are exchange-coupled to each other in a sufficient way, the soft phase possessing the high Ms and the hard phase possessing the high Hc will combine to produce materials exhibiting a superior magnetic property.

The majority of the reported techniques are technically complicated due to the requirement of high sintering temperatures, several steps and separate preparation reactions for each phase before reacting [12,13]. For the effective synthesis of an exchange spring magnet, a high level of homogeneity between hard and soft ferrite phases must be achieved. One possible way targeting that condition is to grow both phases together in a single reaction. This method is called *one-pot* synthetic route, which was first reported by Hazra et al, used to prepare $(NiFe_2O_4)_x/(BaFe_{12}O_{19})_{1-x}$ composites in a simple way [14]. Up to now, some papers presented the synthesis of hard/soft ferrites nanocomposites such as Ba hexaferrite and NiZn ferrites [15], $SrFe_{12}O_{19}$-$Zn_{0.5}Ni_{0.5}Fe_2O_4$ [16], $NiFe_2O_4$-$BaFe_{12}O_{19}$ [17], $SrTm_{0.01}Tb_{0.01}Fe_{11.98}O_{19}$ and spinel ferrites [18], $SrFe_{12}O_{19}$-$Zn_{0.4}Co_{0.2}Ni_{0.4}Fe_2O_4$ [19]. Unfortunately, the optimum exchange-coupling in hard/soft ferrites is very challenging due to the lack of by-products control [8], and the difficulties of tuning the composition by varying the hard/soft ratios.

Thus, in this study we attempted to comprehend the structural, magnetic and microwave properties of $SrFe_{12}O_{19}/MCe_{0.04}Fe_{1.96}O_4$ (M = Cu, Ni, Mn, Co and Zn) hard/soft nanocomposites fabricated via *one-pot* citrate-gel approach, to achieve an exchange spring magnet.

2. Experimental

The synthesis $SrFe_{12}O_{19}/MCe_{0.04}Fe_{1.96}O_4$ (M = Cu, Ni, Mn, Co and Zn) hard/soft nanocomposites were carried out via *one-pot* citrate-gel combustion approach. Metal nitrates of $Sr(NO_3)_2$, $Fe(NO_3)_3.9H_2O$, $Ce(NO_3)_3.6H_2O$, $Ni(NO_3)_2{\cdot}6H_2O$, $Co(NO_3)_2{\cdot}6H_2O$, $Cu(NO_3)_2{\cdot}6H_2O$), $Zn(NO_3)_2{\cdot}6H_2O$, and $Mn(NO_3)_2{\cdot}6H_2O$ were obtained from Merck and used as received.

Stoichiometric contents of the required metal salts were thawed in a certain amount of H_2O to prepare two solutions of $SrFe_{12}O_{19}$ as hard and $MCe_{0.04}Fe_{1.96}O_4$ (M = Cu, Ni, Mn, Co and Zn) as soft, separately. Finally, the hard and soft solutions and required amount of citric acid were mixed under continuous stirring at a temperature of 75 °C. The pH of the solution was arranged to be 7 by adding ammonia solution. The mixtures then were reheated up at 150 °C for 45 min before raising the temperate to 350 °C to generate viscous gels which were burned to get black powder. The residuals were then calcinated at 1000 °C for 5 h [20,21]. Rigaku X-ray diffractometer (XRD) has been used to verify the structure of both hard and soft nanocomposite. Scanning (SEM) and Transmission (TEM) electron microscopy observations were done via FEI Teneo microscope. Magnetic measurements were done via Quantum Design PPMS DynaCool-9 coupled with a head of vibrating sample magnetometer (VSM). Agilent vector network analyzer was used to determine the electromagnetic parameters of the investigated composites between 2 and 18 GHz frequencies range via the transmission line method. The measured reflection coefficient (S_{11}) and transmission coefficient (S_{21}) of the samples were converted into real parts and imaginary parts of permeability ($\dot{\mu}\prime$, $\dot{\mu}''$ and permittivity ($\dot{\varepsilon}\prime$ and $\dot{\varepsilon}''$) which were calculated via Nicholson-Ross-Weir algorithm from recording S-parameters as function of frequencies [22–24].

3. Results and discussion

3.1. Structure

Fig. 1 shows PXRD patterns for $SrFe_{12}O_{19}/MCe_{0.04}Fe_{1.96}O_4$ (M = Cu, Ni, Mn, Co and Zn) hard/soft nanocomposites. The results confirmed the presence of both M-type Sr-hexaferrite JCPDS Card 00-043-0002 and spinel ferrite phases without any occurrence of an external phase, which proves the effectiveness of preparation method to produce a homogeny hard /soft phase. Furthermore, all (114) and (107) peaks for M-type Sr hexaferrite showed great intensity, while the (311) peak of spinel ferrites is fluctuating in response to the type of spinel.

Table 1 – The structural parameters of the hard and soft phases $SrFe_{12}O_{19}/MCe_{0.04}Fe_{1.96}O_4$ (M = Ni, Co, Cu, Mn, and Zn) hard/soft nanocomposites.

Nanocomposite	D_{XRD} (nm)		Hard phase		Soft phase
	Soft	Hard	a = b (Å)	c (Å)	a = b=c (Å)
$SrFe_{12}O_{19}/CoCe_{0.04}Fe_{1.96}O_4$	20.8	36.2	5.8778	23.0115	8.4022
$SrFe_{12}O_{19}/NiCe_{0.04}Fe_{1.96}O_4$	28.8	35.4	5.8870	23.0355	8.3423
$SrFe_{12}O_{19}/ZnCe_{0.04}Fe_{1.96}O_4$	29.2	44.2	5.8848	23.0358	8.4411
$SrFe_{12}O_{19}/CuCe_{0.04}Fe_{1.96}O_4$	21.3	42.6	5.8823	23.0276	8.3344
$SrFe_{12}O_{19}/MnCe_{0.04}Fe_{1.96}O_4$	18.2	26.8	5.8884	23.0243	8.3051

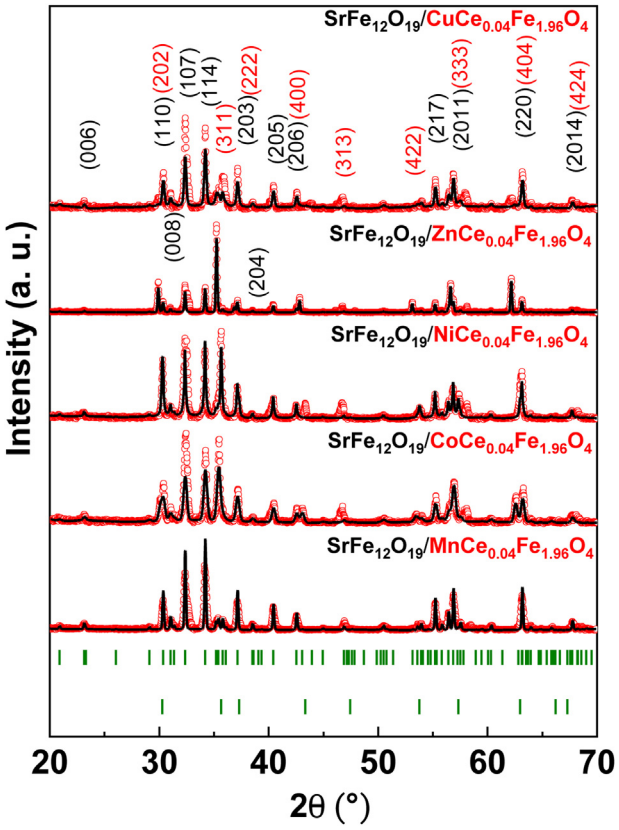

Fig. 1 – XRD powder patterns of various $SrFe_{12}O_{19}/MCe_{0.04}Fe_{1.96}O_4$ (M = Ni, Co, Cu, Mn, and Zn) hard/soft nanocomposites.

The $MCe_{0.04}Fe_{1.96}O_4$ (M = Ni, Co, Cu, Mn, and Zn) peaks are broadened, which indicate the smaller crystallite sizes. The crystallites size and cell constants of hard/soft nanocomposites have been computed via Rietveld refinement using Match 3! Full proof software. The crystallites sizes of both soft and hard phases are estimated via Scherrer's equation considering the (114) and (311) peaks in the PXRD patterns for all hard and soft nanocomposites. The obtained results are listed in Table 1.

3.2. *Morphology*

The micrographs $SrFe_{12}O_{19}/MCe_{0.04}Fe_{1.96}O_4$ (M = Cu, Ni, Mn, Co and Zn) hard/soft nanocomposites are exhibited in Fig. 2. All compositions showed hexagonal platelet structure for the hard component with some accumulation of spherical grains

Table 2 – The deduced magnetic parameters for all synthesized hard/soft $SrFe_{12}O_{19}/MCe_{0.04}Fe_{1.96}O_4$ (M = Ni, Co, Cu, Mn, and Zn) hard/soft nanocomposites.

Hard/Soft nanocomposites	SQR		n_B (μ_B)	
	300 K	10 K	300 K	10 K
$SrFe_{12}O_{19}/NiCe_{0.04}Fe_{1.96}O_4$	0.478	0.464	10.26	13.73
$SrFe_{12}O_{19}/CoCe_{0.04}Fe_{1.96}O_4$	0.466	0.541	12.36	16.38
$SrFe_{12}O_{19}/CuCe_{0.04}Fe_{1.96}O_4$	0.527	0.501	9.97	12.35
$SrFe_{12}O_{19}/MnCe_{0.04}Fe_{1.96}O_4$	0.582	0.574	12.76	18.37
$SrFe_{12}O_{19}/ZnCe_{0.04}Fe_{1.96}O_4$	0.415	0.251	5.47	8.75

of soft component on the surface of the hexagonal plate due to the interactions of magneto-dipole among the particles. The grains size of soft ferrites is lower than that of hexaferrite phase. Moreover, the morphologies are different according to the type and ionic radii of each spinel ferrite. Fig. 3 presented EDX and elemental mapping of $SrFe_{12}O_{19}/MCe_{0.04}Fe_{1.96}O_4$ (M = Ni and Mn) hard/soft nanocomposites. The graphs confirmed the stoichiometry of prepared hard and soft ferrites. TEM images of $SrFe_{12}O_{19}/MCe_{0.04}Fe_{1.96}O_4$ hard/soft nanocomposites (M = Ni and Zn) are revealed large hexagonal particles with small particles distributed over them as seen from Fig. 4. To prove the formation of both hard and soft phases, the HR-TEM images were employed to determine the interplanar distances as followed 0.25, 0.29, 0.30, 0.042, 0.46, 0.49, 0.50 matching with (311), (220), (106),(103), (102), (101) and (100) that correlated with hexagonal and spinel ferrites. These values are corresponding to the XRD results.

3.3. *Magnetic properties*

The high coercivity (H_c) value of pure hard $SrFe_{12}O_{19}$ hexaferrite and the good magnetic properties (such as high saturation magnetization (M_s)) of pure soft spinel ferrites. The grouping of these two initial phases is appropriate to form exchange-spring coupled nanocomposites. In the present study, we explore the magnetic features and exchange-spring behavior of nanocomposite samples of hard $SrFe_{12}O_{19}$ hexaferrite combined with different soft spinel ferrites. For that purpose, magnetic hysteresis loops were measured under an applied field of ±70 kOe at RT and low temperature. Fig. 5 displays the curves of magnetization plotted against applied magnetic field (*M-H*) for $SrFe_{12}O_{19}/MCe_{0.04}Fe_{1.96}O_4$ (M = Ni and Mn). The magnetic parameters involve M_s, M_r, M_r/M_s ratio and H_c were deduced (see Fig. 5 and Table 2). $SrFe_{12}O_{19}$ HF sample showed ferrimagnetic behavior at both measured temperatures of T = 300 and 10 K. H_c values are about 4340 and 2810 Oe at 300 and 10 K, respectively [25–27]. M_s and M_r values are found be

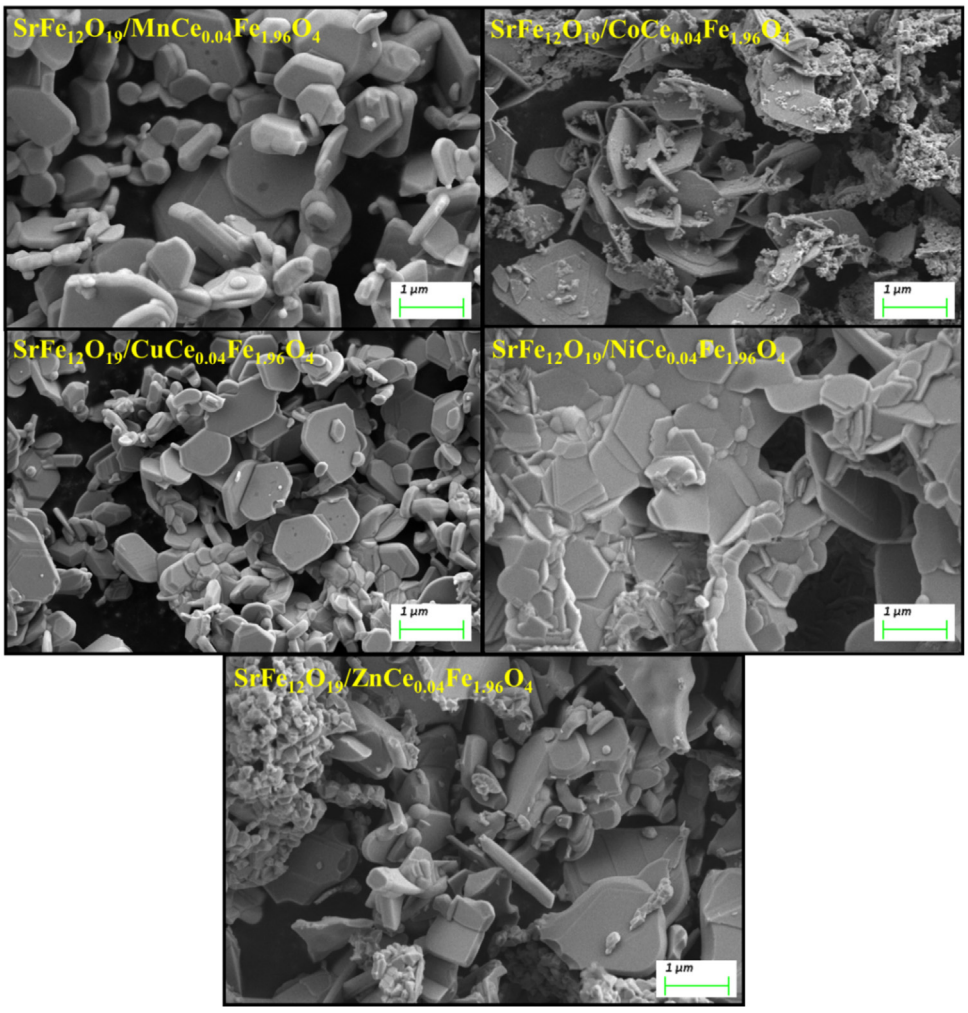

Fig. 2 – SEM images of various $SrFe_{12}O_{19}/MCe_{0.04}Fe_{1.96}O_4$ (M = Ni, Co, Cu, Mn, and Zn) hard/soft nanocomposites.

around 68.5 and 34.8 emu/g at 300 K and 102.5 and 49.9 emu/g at 10 K. The main aspect that is pronounced in various *M-H* curves for nanocomposite samples is the shape of hysteresis loops (see Fig. 5(b) and (d)). Some synthesized samples showed well-smoothed *M-H* loops, which indicate the collaborative swapping of the two interacting phases magnetism via great exchange-coupling among the soft and hard boundaries. The magnetic moments of soft phase turn in line with hard phase as a response to external magnetic field. Consequently, the magnetization and demagnetization of magnets possess the features of a single ferrimagnetic phase [28]. On other hand, some *M-H* loops are not well-smoothed and some of them exhibit kink, which indicates a separable swapping of soft and hard magnetic phases because of uncompleted exchange-coupling among them and thus, a superimposition of two loops will be noticed [28]. Certain levels of dipolar interactions are existing into any produced hard/soft composites owing to hard/hard and soft/soft interactions. However, the influences of interactions on magnetic features could be significant or negligible. Accordingly, the exchange-coupling strength of the composites might be better assessed through exploring dM/dH vs. H curves as shown in Fig. 6 [29,30]. Largely, an excellent exchange-coupling is achieved when a single peak is observed. However, a week or uncoupled exchange will give rise to manifestation of two distinctive peaks. *dM/dH* plots of the two $SrFe_{12}O_{19}/NiCe_{0.04}Fe_{1.96}O_4$ and $SrFe_{12}O_{19}/CoCe_{0.04}Fe_{1.96}O_4$ hard/soft nanocomposites showed two distinct peaks at both measured temperatures, which implies the non-achievable reversal magnetization by one stage. This proves the occurrence of weak exchange-coupling effect in the two $SrFe_{12}O_{19}/NiCe_{0.04}Fe_{1.96}O_4$ and $SrFe_{12}O_{19}/CoCe_{0.04}Fe_{1.96}O_4$ hard/soft nanocomposite phases. At lower temperature, the intensity of the second observed peak slightly reduced and become like a shoulder, which is mostly assigned to the reduced thermal fluctuations. On the other hand, the *dM/dH* plots of other $SrFe_{12}O_{19}/CuCe_{0.04}Fe_{1.96}O_4$, $SrFe_{12}O_{19}/MnCe_{0.04}Fe_{1.96}O_4$ and $SrFe_{12}O_{19}/ZnCe_{0.04}Fe_{1.96}O_4$ hard/soft nanocomposites showed only a single peak, suggesting the achievement of reversal magnetization in one-stage. This reveals the manifestation of good exchange-coupling behavior, which in turn could generate significant influences on magnetic features of hard/soft composites as they attempt to align the both phases magnetic moments to be parallel to each other.

Fig. 7 shows the evolutions in M_s, M_r and H_c values for various prepared products with respect to different spinel

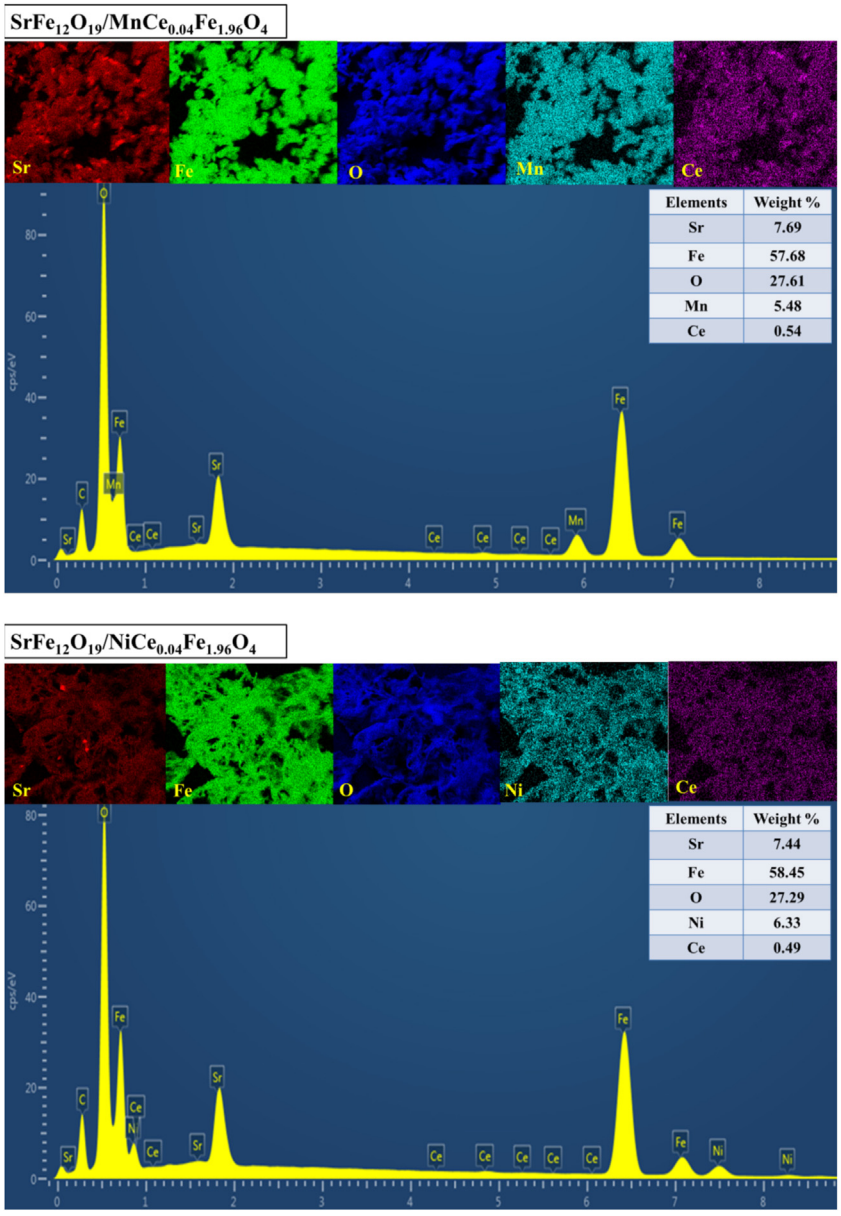

Fig. 3 – EDX spectra and Elemental mappings of $SrFe_{12}O_{19}/MCe_{0.04}Fe_{1.96}O_4$ (M = Ni and Mn) hard/soft nanocomposites.

ferrite phases. It is well-known that M_s and M_r magnitudes are improved at low temperatures compared to the ones at RT. It is principally initiated by the thermal fluctuations' reduction at lower temperatures and thus strengthening the super-exchange interactions among different sites [31–33]. The $SrFe_{12}O_{19}/MCe_{0.04}Fe_{1.96}O_4$ hard/soft composites showed ferrimagnetic behaviors at the both measured temperatures. Furthermore, the specific M_s and M_r magnitudes found in the current study are greater than several earlier investigations of hard Sr hexaferrite and soft spinel ferrites [34–36]. At both temperatures, the maximum M_s and M_r values are for $SrFe_{12}O_{19}/MnCe_{0.04}Fe_{1.96}O_4$ with M_s values of 55 and 79.2 emu/g at RT and T = 10 K, respectively, and M_r values of 32.0 and 45.5 emu/g at T = 300 and 10 K, respectively. M_s and M_r are decreased in $SrFe_{12}O_{19}/CoCe_{0.04}Fe_{1.96}O_4$ to 53.1 and 24.8 emu/g at RT and to 70.4 and 38.1 emu/g at T =10 K, respectively. Then, M_s and M_r are further decreased for $SrFe_{12}O_{19}/NiCe_{0.04}Fe_{1.96}O_4$ and $SrFe_{12}O_{19}/CuCe_{0.04}Fe_{1.96}O_4$. The lowest M_s and M_r values are associated to the $SrFe_{12}O_{19}/ZnCe_{0.04}Fe_{1.96}O_4$ sample, where M_s values are 23.4 and 37.4 emu/g at RT and 10 K, respectively, and M_r values are 9.2 and 9.7 emu/g at RT and 10 K, respectively. Accordingly, the variation tendency in M_s and M_r magnitudes at RT and 10 K from the highest to the lowest for the different synthesized hard/soft nanocomposites can be summarized as follow; $SrFe_{12}O_{19}/MnCe_{0.04}Fe_{1.96}O_4$ > $SrFe_{12}O_{19}/CoCe_{0.04}Fe_{1.96}O_4$ > $SrFe_{12}O_{19}/NiCe_{0.04}Fe_{1.96}O_4$ > $SrFe_{12}O_{19}/CuCe_{0.04}Fe_{1.96}O_4$ > $SrFe_{12}O_{19}/ZnCe_{0.04}Fe_{1.96}O_4$. Without exception, it is evident the existence of sound correlation among the magnetic moments of various M ions and the magnetization, which are as follow $n_{Mn2+} = 5.91\ \mu_B$) > $n_{Co2+} = 3.45\ \mu_B$) > $n_{Ni2+} = 2.44\ \mu_B$ > $n_{Cu2+} = 1.73\ \mu_B$ > $n_{Zn2+} = 0\ \mu_B$. Among diverse synthesized

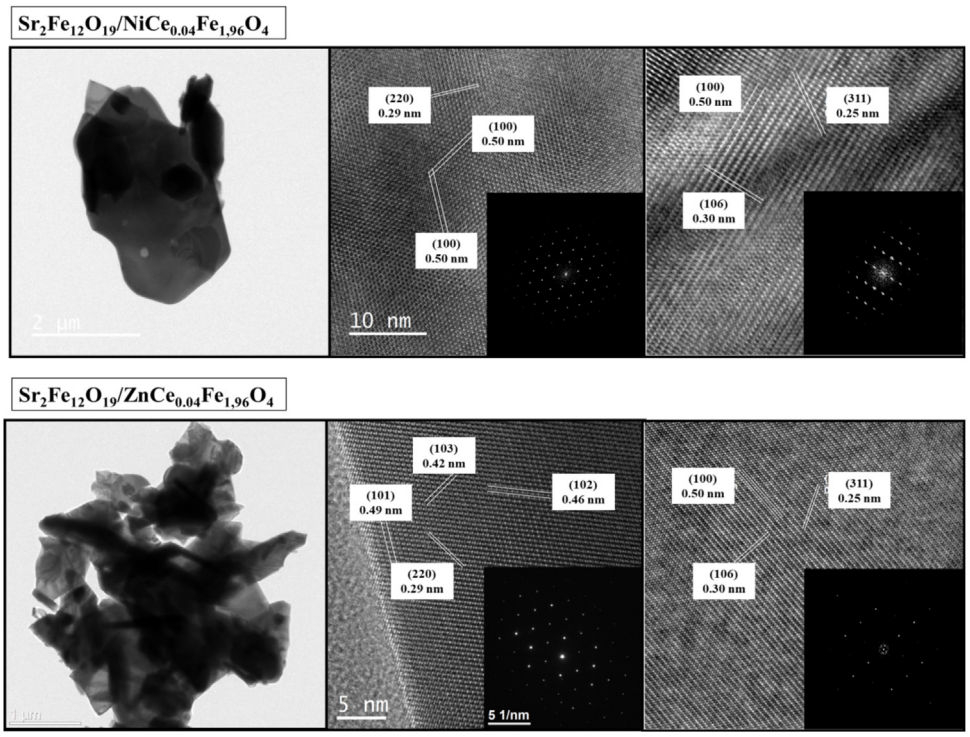

Fig. 4 – TEM and HR-TEM images of various $SrFe_{12}O_{19}/MCe_{0.04}Fe_{1.96}O_4$ (M = Ni and Zn) hard/soft nanocomposites.

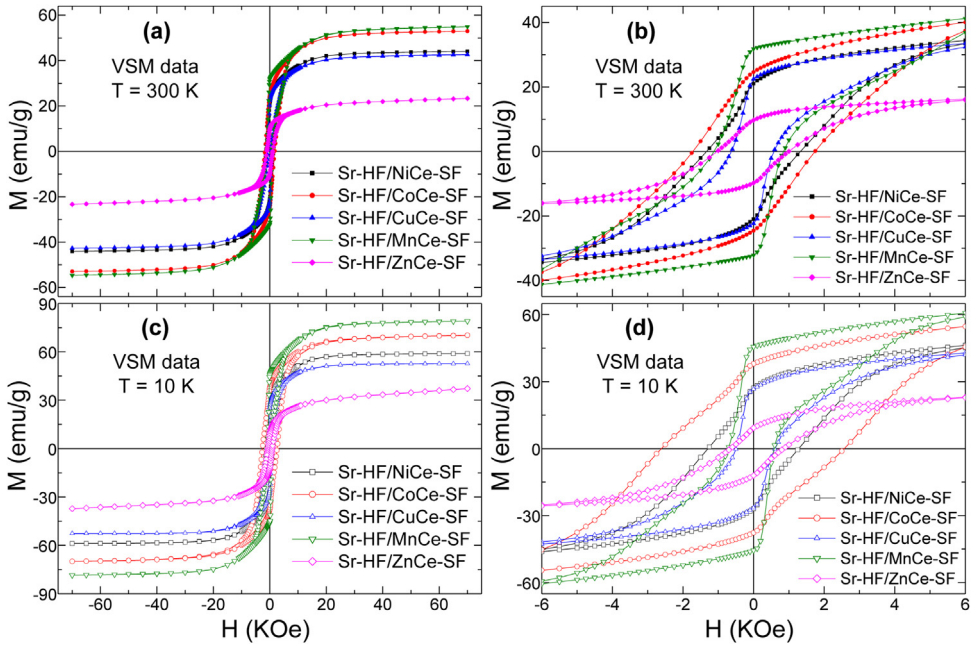

Fig. 5 – M-H hysteresis loops performed at both (a) T = 300 K and (b) T = 10 K for various prepared $SrFe_{12}O_{19}/MCe_{0.04}Fe_{1.96}O_4$ (M = Ni, Co, Cu, Mn, and Zn) hard/soft nanocomposites.

hard/soft nanocomposites, the $SrFe_{12}O_{19}/MnCe_{0.04}Fe_{1.96}O_4$ one resides in a particular place at the nanoscale level. The variations of the microstructure could produce a cations redistribution that will further influence the magnetic features of the nano-ferrites. Mn ferrites are generally known as normal spinel where the tetrahedral A sites are occupied by divalent Mn^{2+} cations, while trivalent Fe^{3+} cations occupy octahedral B sites [37]. Accordingly, Mn normal spinel ferrite barely presents B-B exchange interactions, but no A–A or A–B exchange interactions. By diminishing the size of particles to nanoscale order, a cation inversion happens and hence, the Mn normal spinel ferrite structure is changed to a mixed spinel

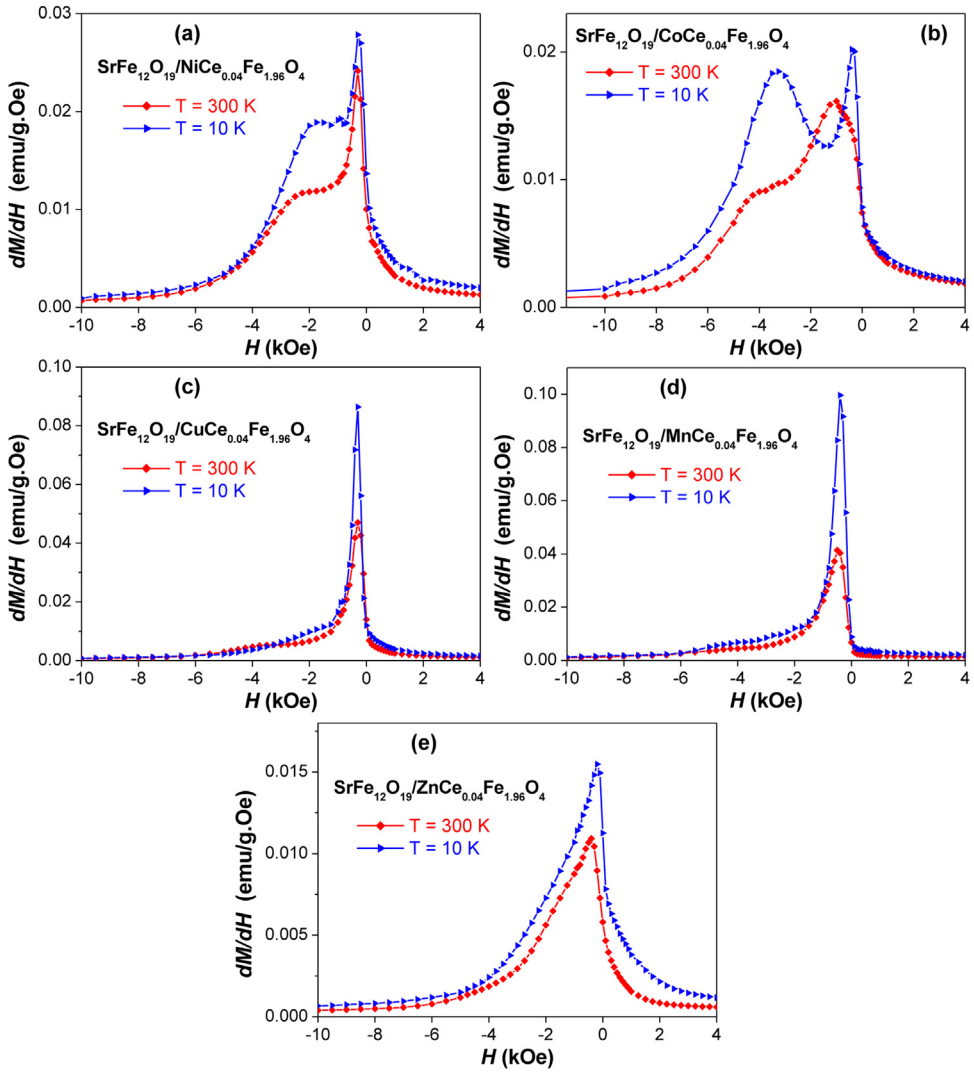

Fig. 6 – *dM/dH vs H* plots performed at RT and 10 K for various prepared $SrFe_{12}O_{19}/MCe_{0.04}Fe_{1.96}O_4$ (M = Ni, Co, Cu, Mn, and Zn) hard/soft nanocomposites.

structure. In this structure, some Fe^{3+} ions are transferred to the A sites and some of the Mn^{2+} ions are transferred to the B sites. As a consequence, the A–B and A–A interactions will be involved along with B–B interactions. The level of cations inversion is increasing with further decreasing the size of particles, and so A–B super-exchange interactions are additionally reinforced, leading to further enhance the magnetic features. This event appears to be apparent in the present occasion of $SrFe_{12}O_{19}/MnCe_{0.04}Fe_{1.96}O_4$ hard/soft nanocomposite. Al Yaqoob and co-workers [38] produced AFe_2O_4 nanoparticles where A = Co, Zn, Ni, and Cu and they explored the magnetic features at 300 K. They indicated that Co and Ni nano-spinel ferrites displayed largely ferromagnetic (FM) behavior, while Cu and Zn nano-spinel ferrites showed superparamagnetic (SPM) behavior. $CoFe_2O_4$ nanoparticles revealed the supreme magnetization and coercivity values amongst others (AFe_2O_4 where A = Ni, Cu or Zn). M_s and M_r magnitudes are decreased from the highest to the lowest as follow $CoFe_2O_4$, $NiFe_2O_4$, $CuFe_2O_4$, and $CuFe_2O_4$, which can explain the evolutions in magnetization values for various prepared hard/soft composites.

As mentioned above, the magnetic moment has an influence on the variation of M_s and M_r values. Accordingly, the magnetic moments (n_B) experimental values are calculated for all synthesized $SrFe_{12}O_{19}/MCe_{0.04}Fe_{1.96}O_4$ nanocomposites by using the following expression [39]:

$$n_B = \frac{M_w \times M_s}{5585}$$

M_w represents the nanocomposite's molecular weight. The n_B calculated values are recorded in Table 2. The n_B fallen with the following trend from the highest to the lowest; $SrFe_{12}O_{19}/MnCe_{0.04}Fe_{1.96}O_4$ > $SrFe_{12}O_{19}/CoCe_{0.04}Fe_{1.96}O_4$ > $SrFe_{12}O_{19}/NiCe_{0.04}Fe_{1.96}O_4$ > $SrFe_{12}O_{19}/CuCe_{0.04}Fe_{1.96}O_4$ > $SrFe_{12}O_{19}/ZnCe_{0.04}Fe_{1.96}O_4$, which is in accordance with that observed in M_s and M_r trend. At both measured temperatures, the experimental n_B values are highest for the $SrFe_{12}O_{19}/MnCe_{0.04}Fe_{1.96}O_4$ nanocomposite sample. This reveal the better super-exchange interactions in the

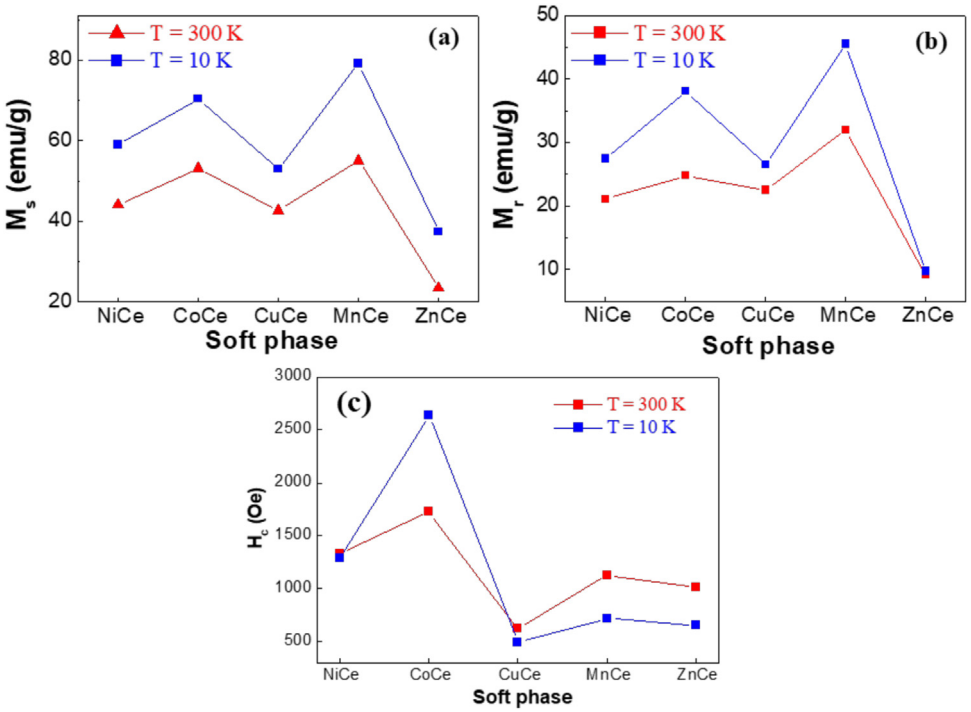

Fig. 7 – Variations in (a) M_s, (b) M_r and (c) H_c for different $SrFe_{12}O_{19}/MCe_{0.04}Fe_{1.96}O_4$ (M = Ni, Co, Cu, Mn, and Zn) hard/soft nanocomposites with respect to various soft nano-spinel ferrite phases.

$SrFe_{12}O_{19}/MnCe_{0.04}Fe_{1.96}O_4$ nanocomposite. The M_r/M_s ratio of all synthesized hard/soft $SrFe_{12}O_{19}/MCe_{0.04}Fe_{1.96}O_4$ (M = Zn, Mn, Cu, Co and Ni) hard/soft composites are recorded in Table 2. Generally, M_r/M_s ratio inferior to 0.5 designates the incompleteness or the exchange-coupling effect [28]. M_r/M_s ratios are smaller than 0.5 are observed in $SrFe_{12}O_{19}/NiCe_{0.04}Fe_{1.96}O_4$, $SrFe_{12}O_{19}/ZnCe_{0.04}Fe_{1.96}O_4$ and $SrFe_{12}O_{19}/CoCe_{0.04}Fe_{1.96}O_4$ hard/soft nanocomposites, reflecting the incomplete or weak exchange-coupling on these products. As the exchange-coupling interaction is a short-range behavior [28], the long-range dipolar interactions among hard and soft phases in these nanocomposites cause the noted decrease in the values of M_r/M_s ratios. On the other hand, the $SrFe_{12}O_{19}/MnCe_{0.04}Fe_{1.96}O_4$ and $SrFe_{12}O_{19}/CuCe_{0.04}Fe_{1.96}O_4$ hard/soft nanocomposites showed M_r/M_s ratios above average of 0.5, revealing greater exchange interactions in these nanocomposites. Hence, the sol-gel auto-combustion procedure in *one-pot* is efficient to accomplish valuable fine grains growth of the hard and soft phases in adjacent vicinity to build exchange-coupling among nanoparticles. The highest M_r/M_s ratio that attained for $SrFe_{12}O_{19}/MnCe_{0.04}Fe_{1.96}O_4$ hard/soft nanocomposite reveals the greatest exchange-coupling. This product displays the highest energy among other prepared nanocomposites.

The variation of H_c values of all synthesized hard/soft nanocomposite samples for the different Ce substituted nano-spinel ferrites are presented in Fig. 7(c). The observed H_c values in different nanocomposite samples are ranging between the magnitudes of pure soft and hard phases, which is appropriate in the exchange-coupled nanomagnets. Highest H_c values correspond to $SrFe_{12}O_{19}/CoCe_{0.04}Fe_{1.96}O_4$ and $SrFe_{12}O_{19}/NiCe_{0.04}Fe_{1.96}O_4$ hard/soft nanocomposites. Largely, the Co and Mn nano-spinel ferrites could display the largest coercivity compared to other spinel ferrites. This is the most reasonable reason for the highest coercivity in these nanocomposites. It seems that the coercivity values of these two nanocomposite samples may be further enhanced if the exchange-coupling behavior was accomplished in one-step. The $SrFe_{12}O_{19}/MnCe_{0.04}Fe_{1.96}O_4$ hard/soft nanocomposite with highest M_s and M_r values showed relatively high coercivity values. The two other $SrFe_{12}O_{19}/ZnCe_{0.04}Fe_{1.96}O_4$ and $SrFe_{12}O_{19}/CuCe_{0.04}Fe_{1.96}O_4$ hard/soft composites display also quite high coercivity magnitudes, which is mostly recognized to the exchange-coupling completeness among soft and hard phases by one-step. Furthermore, it is well-known that the H_c and crystallites size evolutions are inversely proportional [20,40]; H_c grows with diminishing crystallites size and shrinks with increasing crystallites size. An excellent relationship among H_c and D_{XRD} evolutions was observed.

3.4. *Microwave properties*

Utilizing the coaxial transmission line segment to measure the dielectric permittivity and magnetic permeabilities of the $SrFe_{12}O_{19}/MCe_{0.04}Fe_{1.96}O_4$ (M = Zn, Mn, Cu, Co and Ni) hard/soft composites have been performed. Fig. 8 demonstrates frequency dispersions of the imaginary part and real part permittivity for all investigates composites (a-e). It can be seen that the chemical composition (in particular composition of the soft phase) critically influences the value of the permittivity. This is standart situation for complex iron-based oxides [41,42]. Especially, it can be observed for $SrFe_{12}O_{19}/MnCe_{0.04}Fe_{1.96}O_4$ (8c) and $SrFe_{12}O_{19}/NiCe_{0.04}Fe_{1.96}O_4$ (8b) samples.

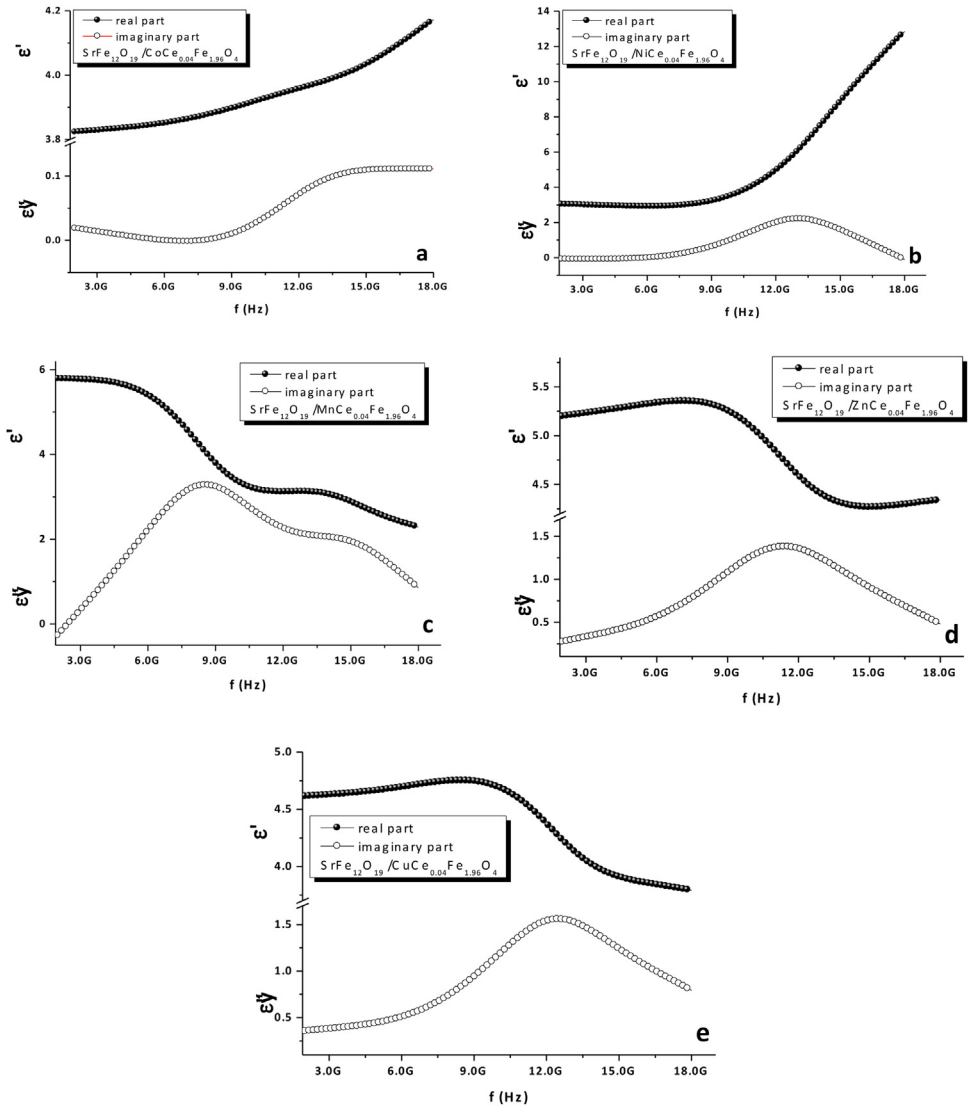

Fig. 8 – Frequency dependencies of the real and imaginary parts of the permittivity of the $SrFe_{12}O_{19}/MCe_{0.04}Fe_{1.96}O_4$ hard/soft nanocomposites, where M = Co (a), Ni (b), Mn (c), Zn (d) and Cu (e)

The values of the real part of permittivity for $SrFe_{12}O_{19}/CoCe_{0.04}Fe_{1.96}O_4$ (8a), $SrFe_{12}O_{19}/ZnCe_{0.04}Fe_{1.96}O_4$ (8d) and $SrFe_{12}O_{19}/CuCe_{0.04}Fe_{1.96}O_4$ (8e) are very similar. Absence of any peaks on frequency dependences of the real part of permittivity confirms the absence of the loss of polarization in this frequency range for $SrFe_{12}O_{19}/MCe_{0.04}Fe_{1.96}O_4$ (M = Co, Mn, Zn and Cu) hard/soft nanocomposites [43]. The rapid increase of the real permittivity for $SrFe_{12}O_{19}/NiCe_{0.04}Fe_{1.96}O_4$ (8b) above 12.3 GHz let us suppose that there is an energy loss on dipole polarization in this frequency range. After analyzing Fig. 8b, we can conclude that there are some broad peaks on curves due to absorption of the high-frequency radiation. The peak position and maximal imaginary permittivity values critically depend on the chemical composition of the $SrFe_{12}O_{19}/MCe_{0.04}Fe_{1.96}O_4$ (M = Zn, Mn, Cu, Co and Ni) hard/soft composites. The main limited parameter is A-site substitution in spinels (M-cation). It can be explained by such factors: **i.** differences in electron shell configuration and radii for A-site ions in spinel; **ii.** features of the AC-charge transport in composites with different microstructure.

At lower frequencies, 2–7 GHz is dominated by the ionic polarization in the material samples. Ionic polarization is origenated from the displacement of the lattice nodes under the action of an external electric field, and the displacement by an amount smaller than the value of the lattice constant [44]. With this polarization, the real part of the dielectric permittivity practically does not change in the frequency range. The imaginary part of the dielectric permittivity gradually diminishes gradually with frequency increasing. In the range from 2 to 12 GHz, there is a transition from ionic polarization to dipole polarization [44].

At frequencies above 12 GHz in $SrFe_{12}O_{19}/MCe_{0.04}Fe_{1.96}O_4$ (M = Ni, Co, Cu, Mn, and Zn) hard/soft nanocomposites are dominated by the dipole polarization. The dipole polarization associated with the dipoles orientation in the external field which is aimed at overcoming the binding forces inside the ions, caused the high losses observed at frequencies less. A

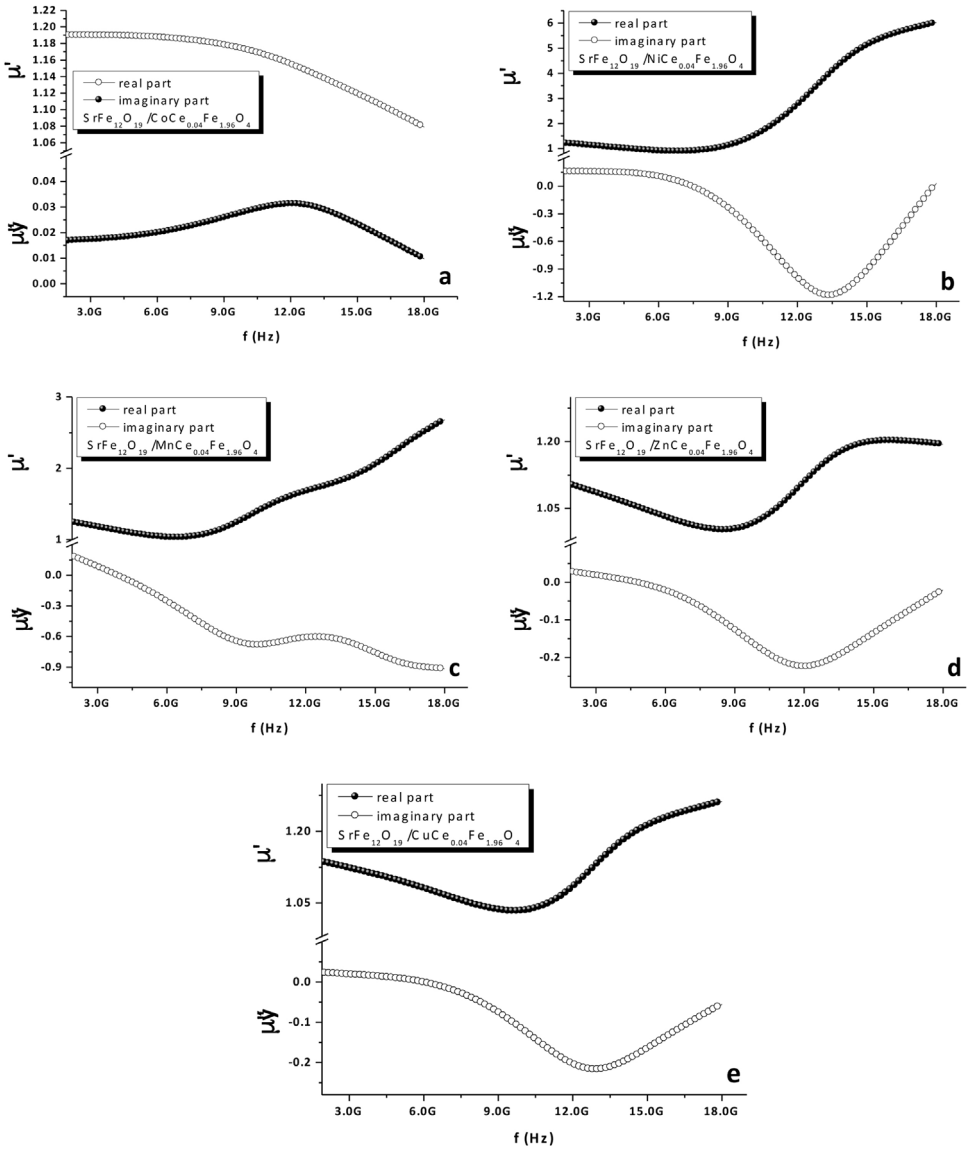

Fig. 9 – Frequency dependencies of the real and imaginary parts of the permeability of the $SrFe_{12}O_{19}/MCe_{0.04}Fe_{1.96}O_4$ hard/soft nanocomposites, where M = Co (a), Ni (b), Mn (c), Zn (d) and Cu (e).

similar change of polarization occurs for other materials but at higher frequencies.

Fig. 9 demonstrates frequency dispersions of the permeability imaginary part real part for all investigates composites. It can be seen that chemical composition (in particular composition of the soft phase) critically influences the value of the permittivity. Especially it can be observed for $SrFe_{12}O_{19}/MnCe_{0.04}Fe_{1.96}O_4$ (9c) and $SrFe_{12}O_{19}/NiCe_{0.04}Fe_{1.96}O_4$ (9b) samples for permeability imaginary and real parts. The values of the real part of permittivity for $SrFe_{12}O_{19}/CoCe_{0.04}Fe_{1.96}O_4$ (9a); $SrFe_{12}O_{19}/ZnCe_{0.04}Fe_{1.96}O_4$ (9d) and $SrFe_{12}O_{19}/CuCe_{0.04}Fe_{1.96}O_4$ (9e) are very similar.

There are some mechanisms for electromagnetic absorption in complex magnetic oxides [45]. One of them is Domain Boundaries Resonance (DBR). Second mechanism concern with Natural Ferromagnetic Resonance (NFR). It is widely known that in the region of the NFR can be observed anomalies in frequency dependences of the permeability imaginary part. Negative values of the permeability imaginary part can be discussed as reflection losses [43].

Based on the imaginary and real parts calculated values of the dielectric permittivity and magnetic permeability, we calculate the reflection coefficient. Fig. 10 demonstrates frequency dependence of reflection coefficient for $SrFe_{12}O_{19}/MCe_{0.04}Fe_{1.96}O_4$ (M = Zn, Mn, Cu, Co and Ni) hard/soft composites in the frequencies of 2-18 GHz.

RL data is well-correlated with the permittivity and the permeability frequency dependence. On the reflection losses frequency dependence (Fig. 10), we can observe non-linear behaviour. Insufficient decrease of the RL in the range up to 7-9 GHz for all samples can be a result of the ionic polarization. Frequency increasing (higher than 9 GHz) lead to changes in the mechanism of EMR absorption. Increase of the RL can be explained by the dipolar polarization. The point of inflexion

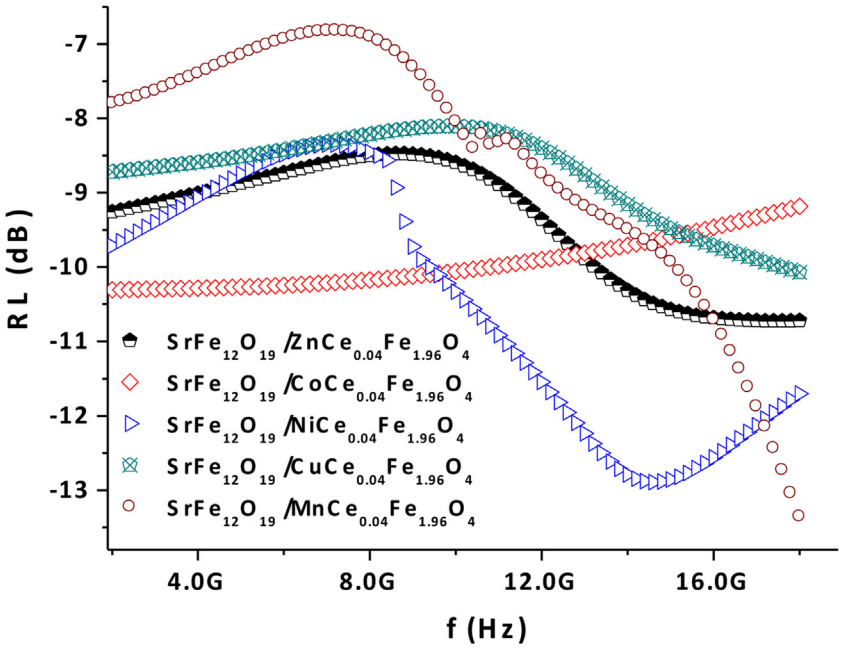

Fig. 10 – Frequency dependencies of the reflection losses (RL) of the $SrFe_{12}O_{19}/MCe_{0.04}Fe_{1.96}O_4$ (M = Ni, Co, Cu, Mn, and Zn) hard/soft nanocomposites.

on the RL curves correspond to the frequency of the transition between two mechanisms. And the position of this point is crucially influenced by the chemical composition of the magnetically soft phase–M-cation in the spinel structure. This can be explained by the configuration of the electronic shell of the A-site cation in spinel.

4. Conclusion

Diversified compositions of $SrFe_{12}O_{19}/MCe_{0.04}Fe_{1.96}O_4$ (M = Zn, Mn, Cu, Co and Ni) hard/soft composites were synthesized utilizing one-pot sol-gel auto-combustion process. The exchange-coupling behavior was investigated in the various synthesized $SrFe_{12}O_{19}/MCe_{0.04}Fe_{1.96}O_4$ (M = Zn, Mn, Cu, Co and Ni) hard/soft composites. The highest exchange-coupling behavior was noticed for the $SrFe_{12}O_{19}/MnCe_{0.04}Fe_{1.96}O_4$ hard/soft nanocomposite. Measurements of the microwave properties of the $SrFe_{12}O_{19}/MCe_{0.04}Fe_{1.96}O_4$ (M = Zn, Mn, Cu, Co and Ni) hard/soft composites were performed using the coaxial method in the frequency range of 2-18 GHz. It was established that the chemical composition (A-site cation in spinel the phase) correlates well with permittivity and permeability. There were two mechanisms proposed for microwave properties explanations: i. ionic polarization (<7 GHz) and ii. dipole polarization (>12 GHz). The point of inflection on the RL curves corresponds to the frequency of the transition between two mechanisms. The position of this point can be explained by the configuration of the electronic shell of the A-site cation in spinel.

Conflict of interest

The authors declare no conflicts of interest.

Acknowledgment

The work was supported by the Russian Science Foundation (agreement number 19-72-10071). Also Authors are thank to the Institute for Research & Medical Consultations (Projects Application No. 2018-IRMC-S-2) of Imam Abdulrahman Bin Faisal University (IAU – Saudi Arabia) for financial and technical supports.

REFERENCES

[1] Dahal JN, Neupane D, Poudel TP. Synthesis and magnetic properties of 4:1 hard-soft $SrFe_{12}O_{19}$-$La_{1-x}Sr_xMnO_3$ nanocomposite prepared by auto-combustion method. AIP Adv 2019;9(7):075308.

[2] Suguna S, Shankar S, Jaganathan SK, Manikandan A. Novel synthesis of spinel $Mn_xCo_{1-x}Al_2O_4$ (x=0.0 to 1.0) nanocatalysts: effect of Mn^{2+} doping on structural, morphological, and opto-magnetic properties. J Supercond Nov Magn 2017;30:691–9.

[3] Hazra S, Ghosh N. Preparation of nanoferrites and their applications. J Nanosci Nanotechnol 2014;14:1983–2000.

[4] Valan MF, Manikandan A, Arul Antony S. Microwave combustion synthesis and characterization studies of magnetic $Zn_{1-x}Cd_xFe_2O_4$ ($0 \leq x \leq 0.5$) nanoparticles. J Nanosci Nanotechnol 2015;15:4543–51.

[5] Pacakova B, Kubickova S, Reznickova A, Niìoanský D, Vejpravova J. Spinel ferrite nanoparticles: correlation of structure and magnetism; 2017.

[6] Manikandan A, Durka M, Seevakan K, Arul Antony S. a novel one-pot combustion synthesis and opto-magnetic properties of magnetically separable spinel $Mn_xMg_{1-x}Fe_2O_4$ ($0.0 \leq x \leq 0.5$) nano photocatalysts. J Supercond Nov Magn 2015;28:1405–16.

[7] Silambarasu A, Manikandan A, Balakrishnan K. Room-temperature superparamagnetism and enhanced

photocatalytic activity of magnetically reusable spinel $ZnFe_2O_4$ nanocatalysts. J Supercond Nov Magn 2017;30:2631–40.
[8] Pan L, Cao D, Jing P, Wang J, Liu Q. A novel method to fabricate $CoFe_2O_4/SrFe_{12}O_{19}$ composite ferrite nanofibers with enhanced exchange-coupling effect. Nanoscale Res Lett 2015;10(1):131.
[9] Ahmad HA, Saiden NM, Saion E, Azis RS, Mamat MS, Hashim M. Effect of PVP as a capping agent in single reaction synthesis of nanocomposite soft/hard ferrite nanoparticles. J Magn Magn Mater 2017;428:219–22.
[10] Kneller EF, Hawig R. The exchange-spring magnet: a new material principle for permanent magnets. IEEE Trans Magn 1991;27, 3588-3560.
[11] Song F, Shen X, Liu M, Xiang J. Magnetic hard/soft nanocomposite ferrite aligned hollow microfibers and remanence enhancement. J Colloid Interface Sci 2011;354:413–6.
[12] Hazra S, Ghosh B, Patra M, Jani R, Vadera S, Ghosh N. One-Pot Synthesis of $(NiFe_2O_4)_x.(SrFe_{12}O_{19})_{1-x}$ Nanocomposites and Their Microwave Absorption Properties. J Nanosci Nanotechnol 2015;15:1–9.
[13] Hazra S, Ghosh BK, Joshi HR, Patra MK, Jani RK, Vadera SR, Ghosh NN. Development of a novel one-pot synthetic method for the preparation of $(Mn_{0.2}Ni_{0.4}Zn_{0.4}Fe_2O_4)_x$–$(BaFe_{12}O_{19})_{1-x}$ nanocomposites and the study of their microwave absorption and magnetic properties. RSC Adv 2014;4(86):45715–25.
[14] Hazra S, Patra M, Vadera S, Ghosh N, Lisjak D. A Novel But Simple "One-Pot" Synthetic Route for Preparation of $(NiFe_2O_4)_x$–$(BaFe_{12}O_{19})_{1-x}$ Composites. J Am Ceram Soc 2012;95:3863–70.
[15] Roy D, Kumar P. Enhancement of (BH)max in a hard-soft-ferrite nanocomposite using exchange spring mechanism. J Appl Phys 2009;106:3902.
[16] Song F, Shen X, Liu M, Xiang J. Preparation and magnetic properties of $SrFe_{12}O_{19}/Ni_{0.5}Zn_{0.5}Fe_2O_4$ nanocomposite ferrite microfibers via sol–gel process. Mat Chem Phys 2011;126:791–6.
[17] Torkian S, Ghasemi A, Shoja Razavi R, Tavoosi M. Structural and magnetic properties of high coercive Al-substituted strontium hexaferrite nanoparticles. J Supercond Nov Magn 2016;29:1627–40.
[18] N.A. Algarou, Y. Slimani, M.A. Almessiere, S. Güner, A. Baykal, I. Ercan, et al., Exchange-coupling effect in hard/soft SrTb0.01Tm0.01Fe11.98O19/AFe2O4 (where A = Co, Ni, Zn, Cu and Mn) composites, Ceram Int., https://doi.org/10.1016/j.ceramint.2019.11.201.
[19] Tavakolinia F, Yousefi M, Afghahi SSS, Baghshahi S, Samadi S. Synthesis of novel hard/soft ferrite composites particles with improved magnetic properties and exchange coupling. Process Appl Ceram 2018;12(3):248–56.
[20] M.A. Almessiere, Y. Slimani, N.A. Tashkandi, H. Güngüneş, M. Sertkol, M. Nawaz, et al., Tailored microstructures, optical and magnetic qualities of strontium hexaferrites: Consequence of Tm3+ and Tb3+ ions Co-substitution, https://doi.org/10.1016/j.ceramint.2019.07.126.
[21] M.A. Almessiere, Y. Slimani, A. Baykal, Synthesis and characterization of $Co1–2xNi_xMn_xCe_yFe_{2-y}O_4$ nanoparticles, https://doi.org/10.1016/j.jre.2019.07.005.
[22] Nicolson AM, Ross GF. Measurement of the intrinsic properties of materials by time-domain techniques. IEEE Trans Instrum Meas 1970;19(4):377–82.
[23] Afsar MN, Birch JR, Clarke RN. The measurement of the properties of materials. IEEE Trans Microw Theor Tech MTT-25 1977;(June).
[24] Klygach DS, Vakhitov MG, Vinnik DA, Bezborodov AV, Gudkova SA, Zhivulin VE, et al. Measurement of permittivity and permeability of barium hexaferrite. J Magn Magn Mater 2018;465:290–4.
[25] Almessiere MA, Slimani Y, Demir Korkmaz A, Güner S, Maarouf AA, Baykal A. Comparative study of sonochemically synthesized Co-Zr and Ni-Zr substituted Sr-hexaferrites: Magnetic and structural investigations. J Magn Magn Mater 2020;497:165996.
[26] Barathiraja C, Manikandan A, Mohideen AMU, Jayasree S. S.A. Magnetically recyclable spinel $Mn_xNi_{1-x}Fe_2O_4$ (x =0.0–0.5) nano-photocatalysts: structural, morphological and opto-magnetic properties. J Supercond Nov Magn 2016;29:477–86.
[27] Padmapriya G, Manikandan A, Krishnasamy V, Jaganathan SK, Arul Antony S. Spinel $Ni_xZn_{1-x}Fe_2O_4$ ($0.0 \leq x \leq 1.0$) nano-photocatalysts: synthesis, characterization and photocatalytic degradation of methylene blue dye. J Mol Struct 2016;1119:39–47.
[28] Torkian S, Ghasemi A. Energy product enhancement in sufficiently exchange-coupled nanocomposite ferrites. J Magn Magn Mater 2019;469:119–27.
[29] Almessiere MA, Slimani Y, Baykal A. Exchange spring magnetic behavior of $Sr_{0.3}Ba_{0.4}Pb_{0.3}Fe_{12}O_{19}/(CuFe_2O_4)_x$ nanocomposites fabricated by a one-pot citrate sol-gel combustion method. J Alloys Compd 2018;762:389–97.
[30] Almessiere MA, Slimani Y, Baykal A. Structural, morphological and magnetic properties of hard/soft $SrFe_{12-x}V_xO_{19}/(Ni_{0.5}Mn_{0.5}Fe_2O_4)_y$ nanocomposites: effect of vanadium substitution. J Alloys Compd 2018;408: 966–75.
[31] Almessiere MA, Slimani Y, Güner S, van Leusen J, Baykal A, Kögerler P. Effect of Nb^{3+} ion substitution on the magnetic properties of $SrFe_{12}O_{19}$ hexaferrites. J Mater Sci: Mater Electron 2019;30:11181–92.
[32] Almessiere MA, Slimani Y, Gungunes H, Manikandan A, Baykal A. Investigation of the effects of Tm^{3+} on the structural, microstructural, optical, and magnetic properties of Sr hexaferrites. Results Phys 2019;13:102166.
[33] Almessiere MA, Slimani Y, El Sayed HS, Baykal A. Morphology and magnetic traits of strontium nanohexaferrites: effects of manganese/yttrium co-substitution. J Rare Earths 2019;37:732–40.
[34] Torkian S, Ghasemi A, Razavi RS. Magnetic properties of hard-soft $SrFe_{10}Al_2O_{19}/Co_{0.8}Ni_{0.2}Fe_2O_4$ ferrite synthesized by one-pot sol–gel auto-combustion. J Magn Magn Mater 2016;416:408–16.
[35] Feng W, Liu H, Hui P, Yang H, Li J, Wang JS. Preparation and properties of $SrFe_{12}O_{19}/ZnFe_2O_4$ core/shell nano-powder microwave absorber. Integr Ferroelectr 2014;152:120–6.
[36] Radmanesh MA, Seyyed Ebrahimi SA. Synthesis and magnetic properties of hard/soft $SrFe_{12}O_{19}/Ni_{0.7}Zn_{0.3}Fe_2O_4$ nanocomposite magnets. J Magn Magn Mater 2012;324:3094–8.
[37] Naseri MG, Saion EB, Kamali A. An overview on nanocrystalline $ZnFe_2O_4$, $MnFe_2O_4$, and $CoFe_2O_4$ synthesized by a thermal treatment method. ISRN Nanotechnol 2012, http://dx.doi.org/10.5402/2012/604241.
[38] Al Yaqoob K, Bououdina M, Akhter MS, Al Najar B, Judith Vijaya J. Selectivity and efficient Pb and Cd ions removal by magnetic MFe_2O_4 (M=Co, Ni, Cu and Zn) nanoparticles. Mater Chem Phys 2019;232:254–64.
[39] Almessiere MA, Demir Korkmaz A, Slimani Y, Nawaz M, Ali S, Baykal A. Magneto-optical properties of rare earth metals substituted Co-Zn spinel nanoferrites. Cer Int 2019;45:3449–58.
[40] Almessiere MA, Slimani Y, Sertkol M, Nawaz M, Baykal A, Ercan I. The impact of Zr substituted Sr hexaferrite: investigation on structure, optic and magnetic properties. Results in Physics 2019;13:102244.

[41] Trukhanov AV, Almessiere MA, Baykal A, Trukhanov SV, Slimani Y, Vinnik DA, et al. Zdorovets Influence of the charge ordering and quantum effects in heterovalent substituted hexaferrites on their microwave characteristics. J Alloy Comp 2019;788:1193–202.
[42] Almessiere MA, Trukhanov AV, Slimani Y, You KY, Trukhanov SV, Trukhanova EL, et al. Correlation between composition and electrodynamics properties in nanocomposites based on hard/soft ferrimagnetics with strong exchange coupling. Nanomaterials 2019;9:202.
[43] Klygach DS, Vakhitov MG, Suvorov PV, Zherebtsov DA, Trukhanov SV, Kozlovskiy AL, et al. Magnetic and microwave properties of carbonyl iron in the high frequency range. J Magn Magn Mater 2019;490:165493.
[44] Klygach DS, Vakhitova MG, Vinnik DA, Bezborodov AV, Gudkova SA, Zhivulin VE, et al. Measurement of permittivity and permeability of barium hexaferrite. J Magn Magn Mater 2018;456:290–4.
[45] Trukhanov AV, Kostishyn VG, Panina LV, Korovushkin VV, Turchenko VA, Thakur P, et al. Control of electromagnetic properties in substituted M-type hexagonal ferrites. J Alloy Comp 2018;754:247–56.